PAN ARCHIVES OF ACOUSTICS
Vol. **42**, No. 4, pp. 697–705 (2017)

DOI: 10.1515/aoa-2017-0072

Sound Scattering by an Elastic Spherical Shell and its Cancellation using a Multi-pole Approach

Eldad Jitzchak AVITAL[(1)], Neeshtha Devi BHOLAH[(1)],
Giuseppe Cortez GIOVANELLI[(2)], Touvia MILOH[(3)]

[(1)] *School of Engineering and Materials Science*
Queen Mary University of London
327 Mile End Road London E1 4NS UK; e-mail: e.avital@qmul.ac.uk, n.d.bholah@se14.qmul.ac.uk

[(2)] *Escoda Politecnica*
Federal University of Rio de Janeiro
Brazil; e-mail: giuseppecg@poli.ufrj.br

[(3)] *School of Engineering*
Tel Aviv University
Ramat Aviv Israel; e-mail: miloh@eng.tau.ac.il

(*received March 11, 2017; accepted August 20, 2017*)

The scattering and transmission of sound by an elastic spherical shell is considered when it is subject to an incoming monochromatic planar wave. It is aimed to cancel the sound scattering using combinations of multi-pole sources located at the centre of a shell filled with compressible fluid. Assuming linear acoustics and structural dynamics, exact solutions are derived for total elimination of the sound scattering for three cases: a free-space, near a hard ground or near a free-surface, where in the last two cases it is assumed that the incoming wave propagates normal to the interface to maximize sound reflection back unto the source of the incoming wave. An elastic spherical shell of 1 m radius embedded in water and filled with air or oil is analysed to show the dominance of low-mode numbers for frequencies of less than 10 kHz and thus demonstrate the ability of this approach to damp acoustic scattering by means of low-order multi-poles inside the shell. Contour and mode distribution plots are also given and analysed.

Keywords: sound scattering; structural dynamics; sound cancellation.

1. Introduction

Sound scattering by a perfectly symmetric sphere is a fundamental topic in acoustics that has attracted significant attention since Lord Rayleigh had presented an analytical solution using a Fourier-Legendre' series for scattering by a rigid (hard) sphere in free-space (Rayleigh, 1945). This topic has a wide range of applications from underwater acoustics (Huang, Gaunaurd, 1997) and room acoustics to particle dynamics control (Barosch *et al.*, 2016). Accounting for the sphere's structural flexibility adds another level of complexity in terms of sound-structure interaction and sound transmission through the structure. A comprehensive analysis for elastic plates, cylindrical and spherical shells acting as sound radiators and scatterers, was given by Junger and Feit (1972) within the framework of linear acoustics and structural dynamics, by employing a Fourier series based approach.

Sound scattering by an elastic spherical shell subject to an incoming planar wave was extended to the case of a shell located near a free-surface or a hard ground (Huang, Gaunaurd, 1997). The image method and the collocation approach were pursued by building elements on the shell's surface. As in the case of the solution for a plate embedded on a free surface (Avital *et al.*, 2012), a least-square operation had to be used in order to overcome an ill-conditioned matrix derived to compute the amplitudes of the Fourier series of the scattered pressure field. Acoustic scattering by an elastic spherical shell filled with air and located near the seabed or free surface was also pursued by Sessarego *el al.* (2012) to find strong resonance interaction between the shell and the interface which was

located close to it. A similar conclusion was drawn by Avital and Miloh (2015) who presented some practical solutions for cancellation of sound scattering using pressure singularities embedded on the shell's wall.

One important aim of the published studies of sound-scattering studies is to achieve reduction of the scattered sound field or transmitted sound, in order to reduce the acoustic signature and avoid detection. This was usually achieved using passive means, while the new formulation of this study seeks to do so using an active mean of a multi-pole sound-source. Passive means include coating the body with material that will absorb some of the acoustic energy, while minimizing reflection by selecting the surface acoustic impedance to be similar to that of the surrounding medium. Viscoelastic material is commonly used for this purpose in underwater acoustic applications and Partridge (1996) analysed the case of partly coated axisymmetric bodies to show better scattering's reduction at high frequencies in water (>2 kHz). A bi-layer of elastic coating was demonstrated for a cylindrical shell to reduce scattering for a certain target frequency (or range of frequencies) by using an optimization procedure (Dutrion, Simon, 2017). An alternative coating can be achieved by a combination of small cavities and channels acting together as Helmholtz resonators that damp the incoming acoustic energy and reduce reflection. This approach goes back to the World War II era and has recently re-emerged as part of the modern meta-material approach (Meng *et al.*, 2012). An interesting approach of using the Janus sphere concept, where part of the sphere is hard and the other is soft was suggested by Kim *el al.* (2014) to reduce sound scattering, where the soft/hard domain sizes could be altered using the shape memory alloys (SMA) technology. This approach was shown to have the potential of significantly reducing the scattered acoustic energy of the sphere when it is near a free-surface or a hard ground, by masking the sphere as part of the reflection coming from the free-surface or hard interfaces.

Reduction of sound scattering using pressure actuators mounted on the shell's wall and utilizing the linear structural dynamics of the shell, was proposed by Avital and Miloh (2011) for free- surface piercing cylinders, a spherical shell (Avital, Miloh, 2015) and a circular plate embedded on a free-surface (Avital *et al.*, 2012). Analytical solutions were shown to exist for the optimal distribution of the pressure actuators, yielding total elimination of the sound scattering, when assuming linear acoustics. Practically speaking, when using a finite number of pressure actuators the method was shown to have good capability of significantly reducing sound scattering, especially for low to mid-range frequencies, i.e. when the shell is compact or mildly non-compact relative to the incoming wave length. The mathematical rationale of this approach can be found in the source substitution method used to model sound scattering, replacing the body by a distribution of simple sources within the shell (Zannin, 2000). The effect of those simple sources is similar to the effect of the pressure actuators, however the latter affect the sound field not directly as the simple source but indirectly through the structural dynamics of the shell.

Alternatively, the source substitution method can be based on a series of higher-order multi-poles located at the centre of the body (Crighton *et al.*, 1996), and in the case of a rigid sphere this method simply converges to Rayleigh's solution for sound scattering (Rayleigh, 1945). This leads to the aim of this study to achieve reduction of sound scattering using active means by locating a multi-pole source at the centre of the sphere. Such source can be applied as a combination of simple sources located at a very short distance of each other while acting asymmetrically towards each other. Such approach requires the shell to be filled with a compressible fluid and as in the case of the pressure actuators method, it will be shown that there is an exact solution for the forcing multi-poles to yield total cancellation of the sound scattering, However, for practical reasons, the order of those multi-poles can only be finite and low. Therefore special attention will be given to examine the feasibility of using low- order forcing multi-poles at the shell's centre to significantly reduce the scattered acoustic energy, i.e., by at least 10 dB.

Hence the aim of this paper is to present a new formulation to reduce sound scattering using a multi-pole source configuration and evaluate it for an elastic spherical shell in free space or near a free or hard surface.

The following section presents the methodology of the Fourier-Legendre series approach used in this study for an elastic spherical shell embedded in a free-space, near a free-surface or a hard ground that is illustrated in Fig. 1. This is followed by the Results section, including verification cases and analysis of the three scenarios of an elastic shell in free-space, near a free-surface and a hard ground.

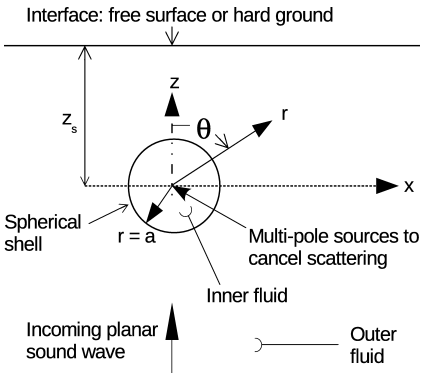

Fig. 1. Schematic description of the problem when the spherical shell is near an interface.

2. Methodology

The governing equations and analytical solutions are derived in this section for a spherical shell as illustrated in Fig. 1. Linear acoustics and structural dynamics are assumed. The incident wave is considered as monochromatic and planar, hence its actual source is assumed to be located far from the shell (Avital, Miloh, 2015; Kim *et al.*, 2014). First the free-space case is considered and then the derivation is extended correspondingly both to the free- surface and hard ground cases.

a. The spherical shell is in free space

Following Kim *et al.* (2014), the sound pressure p_e outside the sphere can be expressed as

$$p_e(x,z,t) = p_0 e^{i(k_e z-\omega t)} + \sum_{n=0}^{N} b_n h_n^{(1)}(k_e r) P_n(\cos\theta) e^{-i\omega t}. \quad (1)$$

The first term on the right hand side of Eq. (1) represents the incident wave pressure and the second term represents the scattered wave pressure. As linear acoustics is assumed, the amplitude p_0 can be taken as unity without losing any generality. The incident wave's propagation direction is z, x is perpendicular to z and t is time. In addition k_e is the wave number, ω is the wave frequency, r is the spherical radius measured from the sphere's centre and θ is the polar angle. Finally, $h_n^{(1)}$ is the spherical Hankel function of the first kind, $P_n(\cos\theta)$ is the Legendre' function and b_n are coefficients to be determined.

The acoustic pressure inside the shell p_i can be accordingly written as

$$p_i(x,z,t) = \sum_{n=0}^{N} c_n j_n^{(1)}(k_i r) P_n(\cos\theta) e^{-i\omega t} + \sum_{n=0}^{N} f_n h_n^{(1)}(k_i r) P_n(\cos\theta) e^{-i\omega t}. \quad (2)$$

The first term on the right hand side of Eq. (2) represents the wave pressure transmitted into the shell's inner fluid and the second the pressure due to the multipoles at the centre of the shell. The wave number in the fluid within the shell is denoted by k_i, j_n is the spherical Bessel function of the first kind. In this study we will match the external sound pressure with the internal one in the Fourier-Legendre space. For this purpose the $\exp(ik_e z)$ function in the incident wave term of Eq. (1) can be expanded as

$$e^{ik_e z} = \sum_{n=0}^{N} (2n+1) i^n j_n(k_e r) P_n(\cos\theta). \quad (3)$$

Similarly the shell's deflection w can also be expressed using a Legendre series;

$$w(\theta,t) = \sum_{n=0}^{N} W_n P_n(\cos\theta) e^{-i\omega t}. \quad (4)$$

By relating the pressure discontinuity across the elastic shell to its radial deflection, one gets

$$W_n = \frac{c_n j_n(k_i a) + f_n h_n^{(1)}(k_i a) - a^*}{i\omega Z_n}, \quad (5)$$

where

$$a^* = [(2n+1) i^n j_n(k_e a) + b_n h_n^{(1)}(k_e a)],$$

and Z_n is the corresponding shell acoustic impedance for mode n and its expression is given in Appendix A. Closure is obtained by enforcing, the dynamic boundary conditions relating the normal derivatives of the external and internal pressures with the shell's deflection (Avital, Miloh, 2011; 2015):

$$\frac{\partial p_e}{\partial r} = -\rho_e \frac{\partial^2 W}{\partial t^2}, \qquad \frac{\partial p_i}{\partial r} = -\rho_i \frac{\partial^2 W}{\partial t^2}, \quad (6)$$

where ρ_e and ρ_i denote the external and internal fluid densities respectively.

Combining Eqs. (5) and (6) leads to the following set of equations:

$$A_{11} b_n + A_{12} c_n + A_{13} f_n = F_1, \quad (7)$$

$$A_{21} b_n + A_{22} c_n + A_{23} f_n = F_2. \quad (8)$$

The expressions for A_{11}, A_{12}, A_{21}, A_{22}, F_1 and F_2 are given in Appendix B. There are three unknowns in Eqs. (7) and (8), the scattered pressure amplitude b_n, the transmitted pressure amplitude c_n and the multipole pressure amplitude f_n. If there are no multi-poles inside the shell, i.e. $f_n = 0$, then b_n and c_n can be determined uniquely. Alternatively, if the scattered amplitude is to be completely cancelled, i.e., $b_n = 0$, then the coefficients c_n and f_n can also be uniquely determined.

b. The spherical shell is near a free-surface or a hard-ground interface

The extension of the free-space derivation to the free surface case follows the methodology of Avital and Miloh (2015). An illustration of the problem is given in Fig. 1. The free surface effect can be modelled by putting an anti-image of the shell above the free-surface. In this derivation we will assume that the incident wave propagates perpendicular to the free surface as in (Avital *et al.*, 2012; Avital, Miloh, 2015; Kim *et al.*, 2014). This is the case where the sound source of the incident wave and the receiver are located at the

same place and the wave is sent perpendicular to the free-surface to maximize reflections propagating back to the receiver. Hence the acoustic pressure $p_{sct,img}$ scattered by the anti-image sphere can be expressed as

$$p_{sct,img}(x,z,t) = -\sum_{n=0}^{N} b_n h_n^{(1)}(k_e r_{img}) \cdot P_n(\cos\theta_{img}) e^{-i\omega t}. \tag{9}$$

However, expression (9) is not convenient as r_{img} and θ_{img} are measured as relative to the centre of the anti-image sphere. Therefore as in (Avital, Miloh, 2015; Kim *et al.*, 2014) a transformation matrix is used to express the scattered pressure as a Legendre' series on the original sphere's surface and relative to its centre:

$$p_{sct,img}(r=a,\theta,t) = \sum_{n=0}^{N} e_n P_n(\cos\theta) e^{-i\omega t}, \qquad e_n = \sum_{j=0}^{N} E_{nj} b_j. \tag{10}$$

Similarly one can express:

$$\frac{\partial p_{sct,img}}{\partial r}(r=a,\theta,t) = \sum_{n=0}^{N} g_n P_n(\cos\theta) e^{-i\omega t}, \qquad g_n = \sum_{j=0}^{N} G_{nj} b_j. \tag{11}$$

The transformation matrices E_{nj} and G_{nj} can be found by calculating the spatial distribution of each mode in Eq. (9) or its radial derivative evaluated on the sphere's surface and decompose it into a Legendre series.

The incident wave can be expressed as

$$p_{inc}(x,z,t) = \sin(k_e(z-z_s))e^{-i\omega t} = \frac{e^{-ik_e z_s}e^{ik_e z} - e^{ik_e z_s}e^{-ik_e z}}{2i} e^{-i\omega t}, \tag{12}$$

where the free surface is at a distance z_s above the sphere's centre. Thus one can modify the free space derivation to include the effect of $p_{sct,img}$ and find the amplitudes of the scattered, transmitted and multi-pole source waves for $\exp(ik_e z)$ and $\exp(-ik_e z)$ separately and then combine them as follows:

$$b_n = \frac{e^{-ik_e z_s} b_n^{(1)} - e^{ik_e z_s} b_n^{(2)}}{2i}, \tag{13}$$

where $b_n^{(1)}$ and $b_n^{(2)}$ are the scattered wave amplitudes for the incident waves $\exp(ik_e z)$ and $\exp(-ik_e z)$ respectively. Similar relations can used for the transmitted wave amplitude c_n and the multi-pole amplitude f_n. The governing equations that account for the presence of the anti-image sphere and the incident wave $\exp(ik_e z)$ are;

$$A_{11} b_n^{(1)} + \sum_{j=0}^{N} \left(G_{nj} - \frac{\rho_e \omega}{Z_n} \right) b_n^{(1)} + A_{12} c_n^{(1)} + A_{13} f_n^{(1)} = F_1, \tag{14}$$

$$A_{21} b_n^{(1)} - \frac{\rho_i \omega}{Z_n} \sum_{j=0}^{N} E_{nj} b_j^{(1)} + A_{22} c_n^{(1)} + A_{23} f_n^{(1)} = F_2. \tag{15}$$

The expressions for A_{11}, A_{12}, A_{21}, A_{22}, F_1 and F_2 are the same as those for the free-space case and are given in Appendix B. Equations (14) and (15) consist of a matrix equation that can be solved using an LU-solver. In order to solve for the case of the incident wave $\exp(-ik_e z)$ one simply has to replace k_e with $-k_e$ in the expressions of Eqs. (14) and (15), yielding the sought equations for $b_n^{(2)}$, $c_n^{(2)}$ and $f_n^{(2)}$.

As in the free-space case, there are two distinct scenarios of interest. The first is without a multi-pole at the centre of the sphere, i.e. $f_n^{(1)} = f_n^{(2)} = 0$ and the second is for a nil scattered wave i.e. $c_n^{(1)} = c_n^{(2)} = 0$. In both scenarios Eqs. (14) and (15) can be solved to determine the rest of the wave amplitudes. The extension for a hard ground is straightforward, instead of an anti-image of the sphere an image of the sphere is used, i.e. the minus sign before the summation operator on the right-hand side of Eq. (9) disappears. The incoming wave is expressed as a standing wave with a cosine distribution instead of the sine distribution in Eq. (12) to reflect that the pressure normal derivative $\partial p/\partial z$ is zero on the interface and not just the pressure as in the free-surface case. Thus, the minus sign on the right hand side of Eq. (13) is replaced by a plus sign and the i disappears from the denominator. The rest of the analysis remains the same.

3. Results and analysis

The Fortran code used for this study is based on earlier published studies (Avital *et al.*, 2012; Avital, Miloh, 2015; Kim *et al.*, 2014). Nevertheless, a verification study is presented in Fig. 2 for the sound scattering by an empty flexible spherical shell that was analytically solved by Junger and Feit (1972). The shell has an Aluminium wall with 5 mm thickness and the sphere's radius is 1 m. The shell is assumed to be embedded in free space of water with ambient density and speed of sound $(\rho_e,\ c_e) = (1000\ \mathrm{kg/m^3},\ 1500\ \mathrm{m/s})$ and the incoming wave frequency is 1500 Hz. A fictitious fluid of a very low acoustic impedance was assumed to be inside the shell for numerical purpose. Very good agreement is obtained

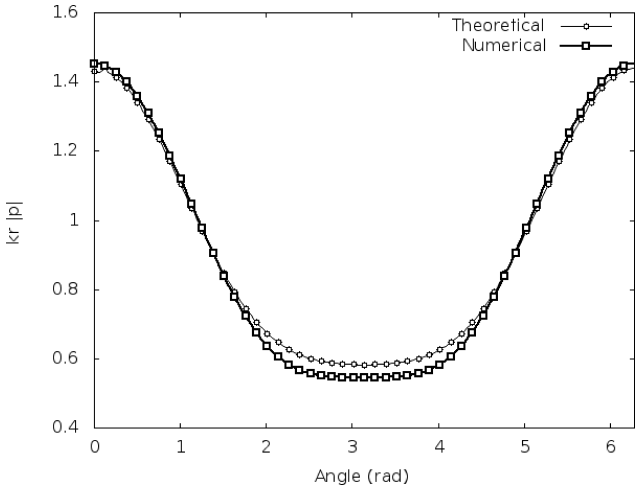

Fig. 2. Far-field pressure directivity verification study, that was calculated for an incoming wave frequency of 1500 Hz and a flexible shell surrounded by water in free space. Theoretically the shell is assumed to be empty and numerically is filled with a fluid of a very low acoustic impedance.

between the numerical and analytical solutions, with a mild difference at the trough of the directivity, which is normal to the incoming propagation path. This is believed to be associated with the inner fluid that is accounted in the numerical solution, but absent in the theoretical solution. Further reducing the acoustic impedance of the inner fluid reduced the difference at the trough of the directivity, but also led to numerical instabilities in calculating high modes. When doing so, one should also be careful not to confuse between the dimensional frequency ω and the non-dimensional frequency Ω of the shell's impedance (see Appendix A) to avoid over-stiffening of the shell (Avital, Miloh, 2015). Other verifications included comparison with Rayleigh's analytical solution for scattered sound by a rigid sphere in free space (Rayleigh, 1945), checking that the pressure behaved as expected at the free-surface and hard ground, i.e. zero pressure and zero pressure gradient respectively, and the pressure distributions at arbitrary points in the sound field fulfilled the Helmholtz equation.

The contours of the scattered and transmitted pressure-amplitude fields are plotted in Fig. 3 for the Aluminium spherical shell of 1 m radius and wall thickness of 5 mm embedded in a free-space surrounded by water. No multi-pole forcing is applied at the centre of the shell to damp the sound scattering. The incoming planar wave propagates at the positive direction of z as in Fig. 1 at frequency of 6000 Hz, i.e. the incoming wave length is 0.25 m. The shell is filled with air in Fig. 3a and oil (octane) in Fig. 3b, where the ambient density and speed of sound are $(\rho_i,\ c_i) = (1.225\ \mathrm{kg/m^3},\ 343\ \mathrm{m/s})$ for air and $(703\ \mathrm{kg/m^3},\ 1171\ \mathrm{m/s})$ for octane. The amplitude of the incoming

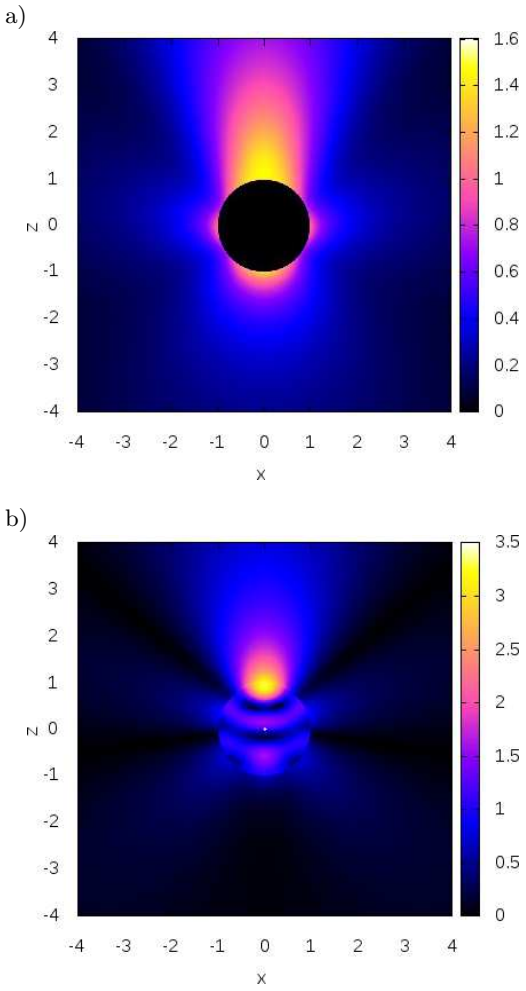

Fig. 3. Scattered near-field pressure-amplitude contours that are plotted for the spherical shell when it is placed in free space of water subject to an incoming wave of 6000 Hz propagating at the z direction. The sphere is a) filled with air and b) filled with oil (octane). No sound forcing is applied at the shell's centre for cancellation of the scattering.

planar wave p was taken as 1 Pa as in all following figures, thus the amplitude contours can be seen as normalised by the amplitude of the incoming wave.

The scattered field creates a wake behind the sphere, which is clearer for the shell filled with air in Fig. 3a. On the other hand, the levels of the transmitted pressure inside the shell are very low as compared to the scattered pressure for the shell filled with air. This is better illustrated in Fig. 4, focusing on the pressure field inside the shell filled by air. Such low pressure levels can be explained by the low acoustic impedance of the air as compared to the water and thus the air's interface with shell behaves similarly to a free-surface, reflecting most of the transmitted sound back into the shell and the water. Standing waves inside the shells of Fig. 4 are revealed with patterns close to spherical and with higher amplitude level on the side that faces the incoming planar wave, i.e. $z \sim -1$ m.

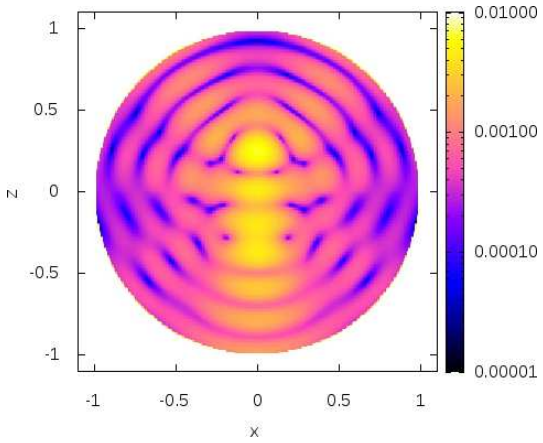

Fig. 4. Transmitted pressure-amplitude contours inside the spherical shell that are plotted for the condition of Fig. 3a.

Changing the inner fluid from air to oil significantly increases the pressure levels, particularly inside the shell as seen in Fig. 3b. This is caused by the better match between the inner and outer fluid acoustic impedances, thus more energy enters the shell and is contained there. A similar finding was made for cylindrical shells filled with a liquid similar to the outer liquid (Avital, Miloh, 2011). It can lead to a shorter scattered wake as more energy is captured by the internal fluid, but on the other hand it can cause resonance effects at certain frequencies, making the shell act more as a radiator than a scatterer (Avital, Miloh, 2011).

The pressure fields caused by the forcing multi-poles when they totally eliminate the externally scattered sound field are plotted in Fig. 5 for the air-filled shell of Fig. 3. It is clearly seen that the pressure fields are dominated by low-order multi-poles, as a source of a few rays of troughs in Fig. 5a, leading to skewed field of an octopole that can be generated by a combination of a dipole and quadrupole. Similar behaviour was observed for the oil-filled shell and thus the following results focus on the air-filled shell. The transmitted pressure contours for the case with forcing multi-poles cancelling the scattered sound are shown in Fig. 6. They are also dominated by low order modes, showing a pattern as of a strong horizontal dipole ($n = 1$) at the centre of the shell surrounded by almost perfect spherical standing waves resembling a monopole-generated ($n = 0$) pressure field in Fig. 6.

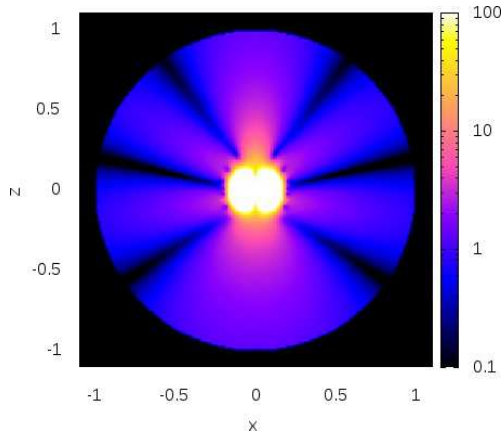

Fig. 5. Pressure-amplitude contours that are due to the forcing multi-poles acting at the centre of the air-filled spherical shell to cancel the external scattered sound field. The rest of the conditions are as in Fig. 3a.

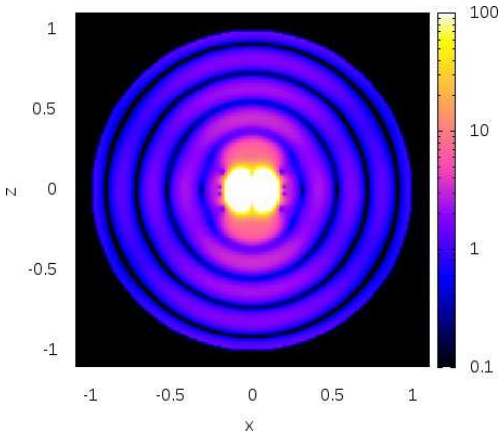

Fig. 6. Transmitted pressure-amplitude contours inside the air-filled spherical shell that are plotted when the multi-poles are acting at the centre of the shell in order to cancel the external scattered sound field. The rest of the conditions are as in Fig. 3a.

The distributions of the modes of the scattered, transmitted and forcing multi-pole source pressures are shown in Fig. 7 for the air-filled shell. Dominance of the low modes is revealed whether the forcing multi-poles are present or not. Auxiliary computations showed that increasing the frequency also increased the order of the dominant modes. The main conclusion from all scattered and forced mode distributions is that they are dominated by low modes which is of importance if we want to achieve a substantial damping of the scat-

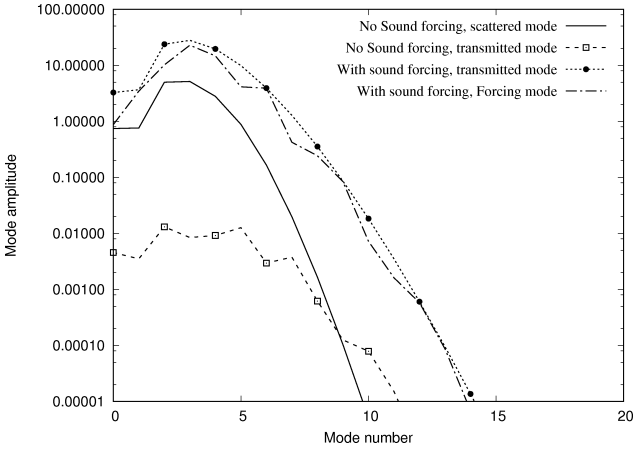

Fig. 7. Sound pressure amplitude modes variation with the mode number that is plotted for the air-filled shell of Fig. 3a in free space and without or with multi-pole sound-source forcing.

tered wave field using low-order multi-poles, a point that will be further discussed at the end of this section.

The effects of hard ground and free-surface, are illustrated in the pressure contour plots of Fig. 8 when subject to an incoming wave frequency of 6000 Hz. No forcing multi-pole was applied to cancel the sound scattering. The distance of 2.1 m between the shell's centre and the interface was chosen to avoid strong resonant standing waves between the shell and the interface. Nevertheless, strong interaction between the shell and the interface is revealed through substantial standing waves as was already discussed in other studies (Sessarego *et al.*, 2012; Avital, Miloh, 2015; Kim *et al.*, 2014). The free-surface enhances the scattered field more than the hard ground as can be seen by comparing Figs 8a with 8b. Nevertheless, both interfaces cause a significant increase in the level of the pressure inside the shell, resulting in an almost uniform distribution of the transmitted pressure. Similar behaviour was also found with the shell having oil inside.

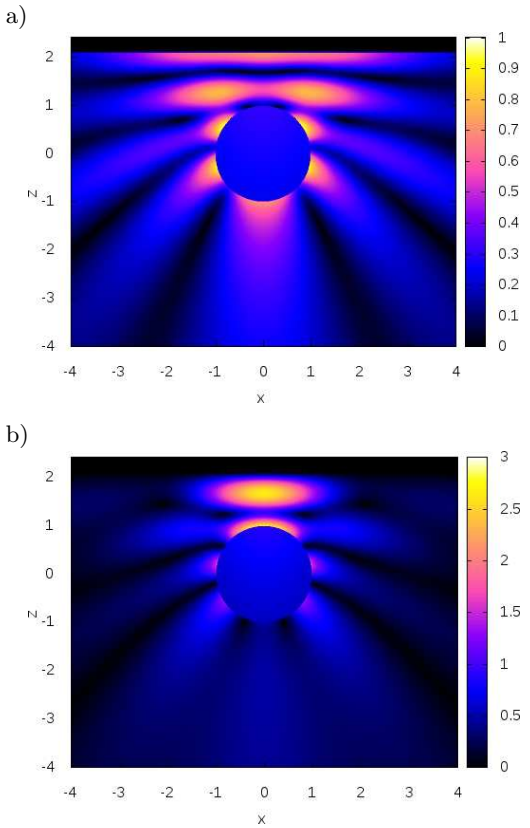

Fig. 8. Scattered near-field pressure-amplitude contours that are plotted for the air-filled spherical surrounded by water and near a) hard ground, and b) free surface at $z = 2.1$ m. The incoming wave frequency is 6000 Hz and there is no forcing at the centre of the shell.

The corresponding pressure fields induced by the forcing multi-poles which are required to eliminate or partially reduce the sound scattering, are shown for the hard interface case in Fig. 9. They show a pattern similar to that seen for the shell in free space of Fig. 5, which is the dominance of low-order multi-poles. The hard ground causes the few radial rays of trough seen in Fig. 5a to disappear.

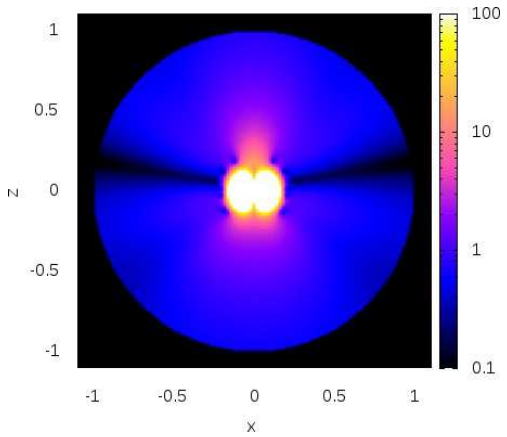

Fig. 9. Pressure-amplitude contours that are due just to the forcing multi-poles acting at the centre of the spherical shell to cancel the external scattered sound field shown in Fig. 8a.

The mode distributions corresponding to the shell of Figs. 8 and 9 are shown in Fig. 10. The distributions are similar to the free space distributions shown in Fig. 7a; (i) the low modes dominate all forms of the sound, i.e. scattered, transmitted and forced, (ii) the amplitude levels are the same as of the free-space and (iii) the forcing multi-poles cause a significant increase in the amplitudes of the transmitted sound. Interestingly, although the modes' amplitude levels of the transmitted sound are at the same level of the free-space case when no forcing is applied , the level of the transmitted pressure inside the shell is much higher

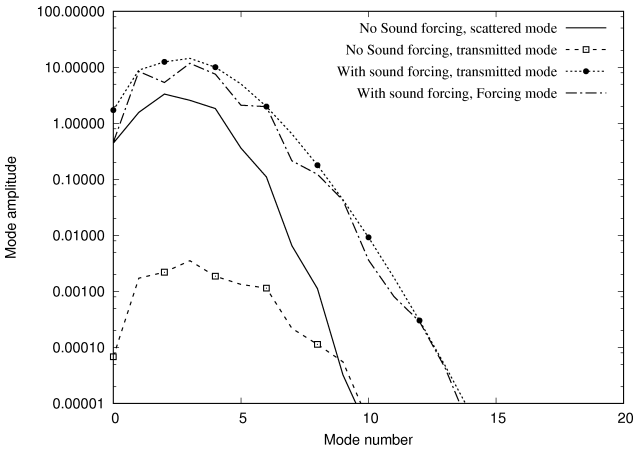

Fig. 10. Sound pressure amplitude modes variation with the mode number that is plotted for the air-filled shell of Fig. 8 near hard ground and without or with multi-pole sound-source forcing.

than in the free- space as can be seen by comparing Fig. 8 with Figs. 4 or 3. This means that the modes of the transmitted pressure are more in phase with others when there is an interface as hard ground or free surface nearby, than when there is none.

To investigate the effect of using a finite number of low-order forcing multipoles to damp the sound scattering, the damping of the scattered acoustic energy in dB as relative to the non-damped energy was calculated as a function of the wave frequency including the highest mode that was cancelled in the scattered noise. This is plotted in Fig. 11 for the air-filled shell in free space and near hard ground. A behaviour close to a linear dependence between the wave frequency and the highest mode of the cancelled scattered sound, is found when gaining a specific damping, say of 10 dB. This is clearer for the free space plot of Fig. 11a, but it is also evident in Fig. 11b for the case of a nearby hard ground. Hence, for 10 dB damping in the scattered acoustic energy one needs to eliminate less than the first five modes of the scattered sound for the wave frequency of 6000 Hz and less than the first fifteen modes for wave frequency of 20 kHz. One should note that in free space there is no dependence between the modes by Eqs. (7) and (8) and thus a clear cut between the damped modes and the non-damped is straightforward. On the other hand, there is an interaction between the modes when an interface is nearby as seen by the matrix Eqs. (14) and (15). Nevertheless, using an optimisation procedure as of Powell, concentration on the low modes is achievable (Avital *et al.*, 2012; Avital, Miloh, 2011; 2015), which is helped by the dominance of the low modes that was seen in the plots of the mode distributions in Figs. 7 and 10.

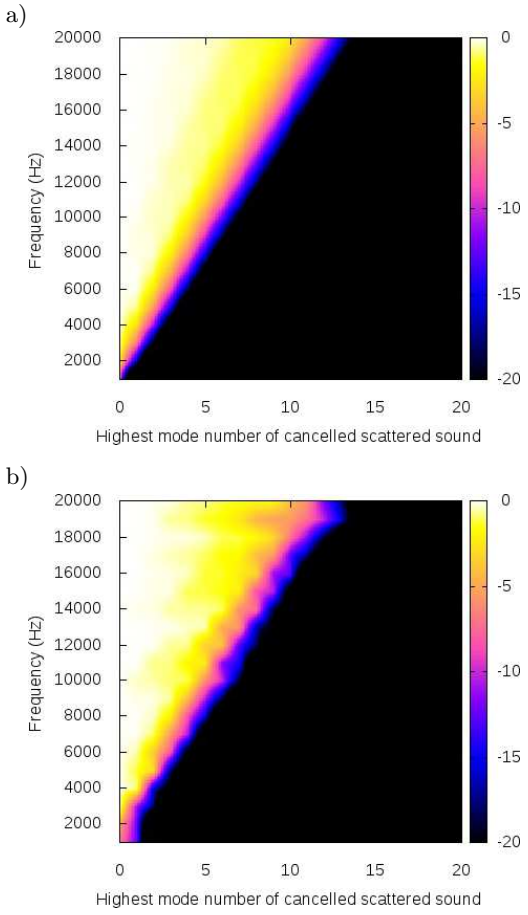

Fig. 11. The variation of the damped scattered energy with the highest mode of sound cancellation for the air-filled shell in a) free space and b) near the hard ground of Fig. 8a.

4. Concluding remarks

Sound scattering by an elastic spherical shell subject to an incoming monochromatic planar wave was analysed using linear acoustics and structural dynamics. The shell's wall was taken as isotropic and homogeneous material. The shell was assumed to be filed with fluid and embedded in free space or near a hard ground or a free-surface. The incoming wave was taken as propagating perpendicular to the interface of hard ground or free surface as to maximize the reflection back to the source of the incoming wave.

The solutions were derived in the Fourier-Legendre space where the method of images was used to account for the effect of an interface as hard ground or free surface. This led to scalar equations for the Fourier-Legendre' modes of the free-space case and matrix equations for the cases of nearby interfaces of hard-ground or free-surface, showing complete independence between the modes for the free-space case and some dependence between the modes for the interface cases.

Three main conclusions can be drawn:

(i) The multi-pole sources located at the centre of the shell can totally eliminate the scattered sound field within the limits of linear theory.

(ii) The sound scattered by the shell and to less extent the sound transmitted into the shell are dominated by low modes. Thus several multi-pole sources located at the centre of the shell can be effective in significantly damping low frequency scattered acoustic energy.

(iii) For higher frequencies when the shell is highly non-compact as relative to the incoming wave length, the high number of modes needed to be damped, makes this approach less attractive as similar to the approach of using pressure actuators mounted on the shell's wall (Avital, Miloh, 2011). Hence the current approach should be combined with a passive approach such as viscoelastic coating that excels better at high frequencies in order to provide a wide frequency range solution.

Appendix A

The acoustic impedance Z_n of a spherical shell in the Fourier-Legendre space was derived by Junger

and Feit (1972) assuming linear acoustics and structural dynamics, and the shell's material being isotropic and homogeneous. This led to the follow expression:

$$Z_n = -\frac{i\rho_s c_p h[\Omega^2 - (\Omega_n^{(1)})^2][\Omega^2 - (\Omega_n^{(2)})^2]}{\Omega a[\Omega^2 - (1-\beta^2)(\nu + \lambda_n - 1)]}, \quad (16)$$

where ρ_s, h and a are the shell's density, thickness and radius respectively. We also define $\beta^2 = h^2/(12a^2)$, $c_p^2 = E/(\rho_s(1-\nu^2))$ with E representing Young's modulus and ν the Poisson ratio. Using n to denote the mode's number as in Sec 2 and defining $\lambda_n = n(n+1)$, $\Omega = \omega a/c_p$, where it $\Omega_n^{(1)}$ and $\Omega_n^{(2)}$ are the normalized resonance frequencies. The latter are also the positive roots of the following quartic equation:

$$\begin{aligned}\Omega^4 &- [1 + 3\nu + \lambda_n - \beta^2(1 - \nu - \lambda_n^2 - \nu\lambda_n)]\Omega^2 \\ &- (\lambda_n - 2)(1 - \nu^2) \\ &+ \beta^2[\lambda_n^3 - 4\lambda_n^2 + \lambda_n(5 - \nu^2) - 2(1 - \nu^2)] = 0. \quad (17)\end{aligned}$$

The resonant frequencies are defined such that $\Omega_n^{(2)} > \Omega_n^{(1)}$ for $n > 0$, and for $n = 0$ only one resonant frequency exists which is here denoted as $\Omega_0^{(2)}$.

Appendix B

Below we provide the explicit expressions for the coefficients A_{11}, A_{12}, A_{21}, A_{22}, F_1 and F_2 used in Eqs. (7), (8), (14) and (15):

$$A_{11} = k_e h_n^{'(1)}(k_e a) - \frac{i\rho_e\omega}{Z_n} h_n^{(1)}(k_e a), \quad (18)$$

$$A_{12} = \frac{i\rho_e\omega}{Z_n} j_n(k_i a), \quad (19)$$

$$A_{13} = \frac{i\rho_e\omega}{Z_n} h_n^{(1)}(k_i a), \quad (20)$$

$$A_{21} = -\frac{i\rho_i\omega}{Z_n} h_n^{(1)}(k_e a), \quad (21)$$

$$A_{22} = k_i j_n'(k_i a) + \frac{i\rho_i\omega}{Z_n} j_n(k_i a), \quad (22)$$

$$A_{23} = k_i h_n^{'(1)}(k_i a) + \frac{i\rho_i\omega}{Z_n} h_n^{(1)}(k_i a), \quad (23)$$

$$\begin{aligned}F_1 &= -(2n+1) i^n k_e j_n'(k_e a) \\ &\quad + \frac{i\rho_e\omega}{Z_n}(2n+1) i^n j_n(k_e a), \quad (24)\end{aligned}$$

$$F_2 = \frac{i\rho_i\omega}{Z_n}(2n+1) i^n j_n(k_e a). \quad (25)$$

Acknowledgment

Computing time provided by Queen Mary's MidPlus cluster under EPSRC grant EP/k000/28/1 is kindly acknowledged.

References

1. Avital E.J., Korakianitis T., Miloh T. (2012), *Sound scattering by a flexible plate embedded on free surface*, Advances in Acoustics and Vibration, **2012**, Article ID 473531, doi: 10.1155/2012/473531.

2. Avital E.J., Miloh T. (2011), *Sound scattering by free surface piercing and fluid-loaded cylindrical shells*, Philosophical Transactions of the Royal Society A: Mathematical, **369**, 1947, 2852–2863.

3. Avital E.J., Miloh T. (2015), Sound scattering and its cancellation by an elastic spherical shell in free space and near a free surface, *Wave Motion*, **55**, 35–47.

4. Barosch D., Tomas J.L., Marchiano R. (2016), *Observation of a single beam gradient force acoustical trap for elastic particles: acoustical tweezers*, Physical Review Letters, **116**, 2, 024301.

5. Crighton D.G., Dowling A.P., Ffowcs Williams J.E., Heckl M., Leppington F.G. (1996), *Modern methods in analytical acoustics*, Springer-Verlag.

6. Dutrion C., Simon F. (2017), *Acoustic scattering reduction using layers of elastic materials*, Journal of Sound and Vibration, **388**, 53–68.

7. Huang H., Gaunaurd G.C. (1997), *Scattering of a plane acoustic wave by a spherical elastic shell near a free surface*, International Journal of Solids and Structures, **34**, 5, 591–602.

8. Junger M.C., Feit D. (1972), *Sound, structures and their interaction*, MIT Press.

9. Kim D., Avital E.J., Miloh T. (2014), *Sound scattering and its reduction by a Janus sphere type*, Advances in Acoustics and Vibration, **2014**, Article ID 392138, doi: 10.1155/2014/392138.

10. Meng H., Wen J., Zhao H., Wen X. (2012), *Optimisation of locally resonant acoustic metamaterials on underwater sound absorption characteristics*, Journal of Sound and Vibration, **331**, 1, 4406–4416.

11. Partridge C. (1996), *Acoustic scattering from viscoelastically coated bodies*, Journal of the Acoustical Society of America, **99**, 1, 72–78.

12. Rayleigh J.W.S. (1945), *The theory of sound – Volume II*, Dover Publications.

13. Sessarego J.P., Cristine P., Grigorieva N.S., Fridman G.M. (2012), *Acoustic scattering by an elastic spherical shell near the seabed*, Journal of Computational Acoustics, **20**, 3, 1250006.

14. Zannin P.H.T. (2000), *Factors that influence the calculation of acoustic scattering by the method of source simulation*, Archives of Acousics, **25**, 3, 317–329.